ELSEVIER

Chemical Engineering Journal 68 (1997) 51–62

Chemical Engineering Journal

A core–annulus model for the radial flow structure in a liquid–solid circulating fluidized bed (LSCFB)

Wu-Geng Liang, Jing-Xu Zhu *

Department of Chemical and Biochemical Engineering, University of Western Ontario, London, Ont., Canada, N6A 5B9

Received 23 August 1996; revised 21 May 1997; accepted 2 June 1997

Abstract

A core–annulus model is developed to describe the radial nonuniform flow structure in a liquid–solid circulating fluidized bed (LSCFB). Good agreement is obtained between the model predictions and the experimental results of the radial distributions in the bed voidages and liquid velocities under different superficial liquid velocities and particle circulation rates. The variations of the liquid velocity, particle velocity, bed voidage and slip velocity in the core and annular regions are predicted with the model under different superficial liquid velocities and different particle circulation rates. The variation of the radial non-uniformity of the flow structure is also discussed and a mechanistic explanation is presented. A radial uniformity index is proposed to characterize the radial flow structure. The similarities and differences between gas–solid and liquid–solid fluidization systems are compared. © 1997 Published by Elsevier Science S.A.

Keywords: Liquid–solid system; Flow structure; Core–annulus model; Circulating fluidized bed; Radial non-uniformity

1. Introduction

Liquid–solid fluidization is thought traditionally to be homogenous with a spatially uniformly distributed concentration of solid particles [1,2]. This assumption of homogeneous behaviour for the liquid–solid fluidization forms the basis of the theories of liquid–solid fluidization [3–6]. However, experimental results show that under higher liquid velocity and with particle circulation between the bed and the particle storage vessel there is significant non-uniformity in the radial distributions of the bed voidage, and liquid and particle velocities [7]. Due to the radial non-uniformity of the flow structure, significant errors will occur when the empirical relations for conventional liquid–solid fluidization based on homogeneous fluidization are used to describe the non-uniform flow structure in a liquid–solid circulating fluidized bed (LSCFB) [7]. Therefore, new models are needed to describe the non-uniform flow structure in the LSCFB.

The radial non-uniformity of the flow structure has been found in gas–solid circulating fluidized beds in recent years (e.g. Weinstein et al. [8], Zhang et al. [9] and Herb et al. [10]). While it is desirable to establish a two-dimensional model to fully describe the radial flow distribution, the complexity involved in developing such a model has led to only limited success [11]. A more practical way to describe the radial non-uniformity in the gas–solid system is to use the core–annulus model. This method divides the cross-section into two regions, the core and annular regions, and assumes that the flow structures within both regions are uniform. The differences between the two regions are then used to simulate the radial non-uniformity in the flow structure. The core–annulus method has been successfully applied to describe flow structures [12–15], mixing properties [16], and reaction [17] in gas–solid suspension systems.

In this paper, a core–annulus type model is, for the first time, proposed for a liquid–solid system, to simulate the radial flow structure in the liquid–solid circulating fluidized bed. The model prediction is then compared with the experimental results. Finally, the flow behaviours in the LSCFB are discussed based on the predicted results.

2. Core–annulus model

Experimental results in the LSCFB have indicated that there is radial non-uniform distribution of the flow structure, with higher bed voidage, higher liquid velocity and higher particle velocity in the central region of the bed and with lower values of the above variables in the near wall region [7]. Given these flow characteristics, a core–annulus type model will be suitable for describing the flow structure in the LSCFB. The core–annulus model assumes that there are two

* Corresponding author.

PII S1385-8947(97)00065-X

homogeneous flow regions (core and annulus) in the radial direction of the bed, and uses the differences between them to describe the radial non-uniform flow structure in the LSCFB. While this type of model does not provide the precise radial flow structure, it does provide a practical and very useful method to describe the flow structure before a more precise model becomes available. More importantly, the results obtained with the core–annulus model can also be used to predict the behaviour of an LSCFB reactor, so as to provide some key information for the reactor design.

The assumed core–annulus structure for the liquid–solid two phase flow in an LSCFB is presented in Fig. 1. The model is established with the following assumptions.

1. The flow structure in the cross-section in the LSCFB can be divided into a core region with diameter of r_c and an annular region from $r=r_c$ to $r=R$.
2. The fluidization in each of the core and annular regions is homogeneous, i.e. there are uniform solids holdup and uniform liquid and particle velocity distributions in each of the two regions, although the fluidization in the whole cross-section of the bed is not uniform.
3. The liquid in the core region is flowing upwards with a velocity V_{lc} and the liquid in the annulus may flow upwards or downwards with a velocity V_{la} (upwards is positive).
4. The particles in the core region with a solids holdup of $(1-\varepsilon_c)$ are flowing upward with a velocity V_{sc}. The particles in the annular region with a solids holdup of $(1-\varepsilon_a)$ may flow upwards or downwards with a velocity V_{sa} (upwards is positive) depending on the liquid velocity in this region.
5. In each of the core and the annular regions, due to the homogeneous fluidization assumption, the relationship between the liquid and particle velocities satisfies the theory of generalized fluidization developed for conventional homogeneous liquid–solid fluidization [4–6]. That is, in the core region there is

$$\frac{V_{lc}}{U_t}-\frac{V_{sc}}{U_t}=\varepsilon_c^{n-1} \tag{1}$$

and in the annular region there is

$$\frac{V_{la}}{U_t}-\frac{V_{sa}}{U_t}=\varepsilon_a^{n-1} \tag{2}$$

where U_t is the particle terminal velocity and n is the index of the Richardson and Zaki equation [3].

6. In the fully developed flow, there is no net interchange of liquid and particles between the core and annular regions, because of the uniform flow structure in the axial direction of the bed [7,18].

Based on the above assumptions for the flow structure, five more equations (Eqs. (3)–(7)) can be established. The mass balance for the liquid and solids phases between the two regions at a given cross-section provides

$$\varepsilon_c r_c^2 V_{lc}+\varepsilon_a(R^2-r_c^2)V_{la}=R^2U_l \tag{3}$$

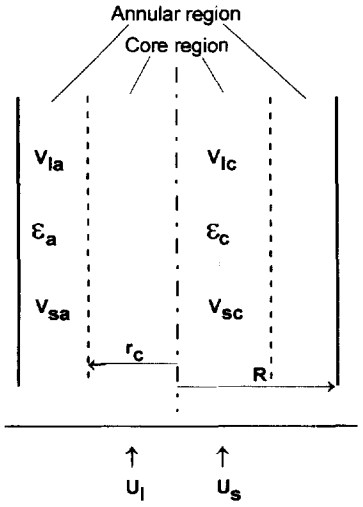

Fig. 1. The core–annulus flow structure of the liquid–solid circulating fluidized bed.

and

$$(1-\varepsilon_c)r_c^2V_{sc}+(1-\varepsilon_a)(R^2-r_c^2)V_{sa}=R^2U_s=R^2G_s/\rho_s \tag{4}$$

where U_l is the superficial liquid velocity, G_s is the particle circulation rate, U_s is the particle circulation rate expressed as superficial particle velocity, and ρ_s is the particle density.

The averaged bed voidage in the two regions should be equal to the bed voidage at this cross-section, that is,

$$r_c^2\varepsilon_c+(R^2-r_c^2)\varepsilon_a=R^2\varepsilon \tag{5}$$

At this cross-section of the bed, the pressure drop across the core region, the annular region and the whole cross-section should be the same because there is no force exerted in the radial direction, so that

$$-\frac{dP}{dx}=\left[-\frac{dP}{dx}\right]_c \tag{6}$$

$$-\frac{dP}{dx}=\left[-\frac{dP}{dx}\right]_a \tag{7}$$

where

$$-\frac{dP}{dx}=(1-\varepsilon)\rho_s g+\varepsilon\rho_l g+\frac{2}{R}(\tau_{lw}+\tau_{sw}) \tag{8}$$

$$\left[-\frac{dP}{dx}\right]_c=(1-\varepsilon_c)\rho_s g+\varepsilon_c\rho_l g+\frac{2}{r_c}(\tau_{lc}+\tau_{sc}) \tag{9}$$

$$\left[-\frac{dP}{dx}\right]_a=(1-\varepsilon_a)\rho_s g+\varepsilon_a\rho_l g-\frac{2r_c}{(R^2-r_c^2)}(\tau_{lc}+\tau_{sc})+\frac{2R}{(R^2-r_c^2)}(\tau_{lw}+\tau_{sw}) \tag{10}$$

where τ_{lw} is the shear force between the liquid phase and the wall, τ_{sw} is the shear force between particles and the wall, τ_{lc} is the shear force of the liquid between the core and annular

regions, and τ_{sc} is the shear force of the solids between the core and annular regions.

The shear forces in Eqs. (8)–(10) are obtained from the following correlations. The shear force between the liquid phase and the wall of the bed is [19]:

$$\tau_{lw}=\frac{1}{2}f_{la}\rho_l\varepsilon_a V_{la}^2 \tag{11}$$

where f_{la} is the Fanning friction factor.

The shear force between the solids phase and the wall is usually correlated with the liquid velocity but not the particle velocity, and has been given as follows [20,21]:

$$\tau_{sw}=\frac{1}{2}f_{sa}\rho_s(1-\varepsilon_a)V_{la}^2 \tag{12}$$

where f_{sa} is the friction factor between the particles and the wall.

The shear force between the core and annular regions is obtained with the assumption that there is a 'wall' between the two regions. Therefore, the equations for the shear forces would have the same forms as Eqs. (11) and (12) but with a different liquid velocity. The difference in the liquid velocities between the two regions is used instead of V_{la}. Therefore, the shear forces of liquid and solids phases between the core and annular regions are:

$$\tau_{lc}=\frac{1}{2}f_{lc}\rho_l\varepsilon_c(V_{lc}-V_{la})^2 \tag{13}$$

$$\tau_{sc}=\frac{1}{2}f_{sc}\rho_s(1-\varepsilon_c)(V_{lc}-V_{la})^2 \tag{14}$$

where f_{lc} is the Fanning friction factor of the liquid phase between the core and the annular regions and f_{sc} is the friction factor of the solids phase between the core and the annular regions.

The friction factors in Eqs. (11) and (13) are determined from the Fanning friction factor. Under the operating conditions of our experiments [7] and model prediction, the Fanning friction factor can be obtained based on the Reynolds number [19].

The friction factor between the particles and the wall, f_{sa}, is usually correlated by the following equation [20,21]:

$$f_{sa}=f_0\left(\frac{V_l^2}{gD}\right)^b \tag{15}$$

where D is the diameter of the column, V_l is the liquid velocity, and f_0 and b are the empirical coefficients for the specific system. With the published correlations for liquid–solid transport systems [20,21], f_{sa} and b can be obtained. Substituting V_l with V_{la} or $(V_{lc}-V_{la})$ and D with $2R$ or $2r_c$, the solids friction factors between the annulus and the wall and between the core and annular regions can be obtained.

There are seven variables in the flow model (V_{lc}, V_{la}, V_{sc}, V_{sa}, ε_c, ε_a and r_c) and there are also seven independent equations (Eqs. (1)–(7)), so that the seven variables can be obtained for different operating conditions. Model inputs are U_l, U_s, ε and the physical properties of the liquid and particles. All other conditions are normally given except ε, which needs to be obtained experimentally.

3. Comparison of model predictions with experimental results

With the core–annulus model proposed above, the variables in the core and annular regions can be obtained for a given set of specific operating conditions, that is, with the known U_l, U_s and ε and the liquid and particle properties. In order to compare the predicted results with the experimental results of Liang et al. [7], the diameter of the circulating fluidized bed for the model prediction is chosen as 0.14 m, the same as in the experiments. The properties of the liquid and solids phases for the model predictions are also the same as those in the experiments: the liquid phase is tap water and the solids phase is glass beads with a diameter of 0.405 mm and a density of 2460 kg m^{-3}. The terminal velocity for this particle is 0.053 m s^{-1}. The operating ranges of the variables for the model prediction are also chosen to be the same as those of the experiments, that is, the superficial liquid velocity is in the range of 0.051 to 0.135 m s^{-1}, and the particle circulation rate is from 0.0 to 0.0015 m s^{-1}.

The predicted cross-section radial flow structure under $U_l=0.077$ m s^{-1}, $U_s=0.0011$ m s^{-1} and $\varepsilon=0.914$ is given in Fig. 2. The experimental radial bed voidage and liquid velocity distributions under the same operating conditions are given in the same figure. It can be seen that the predicted bed voidages and liquid velocities are consistent with the experimental results: the predicted results indicate that in the LSCFB, the flow structure is non-uniform in the radial direction. The bed voidage, liquid velocity and particle velocity are higher in the core region, and lower in the annular region. Liquid and particles move upward in the core region. Liquid and particles also move upward in the annulus under these

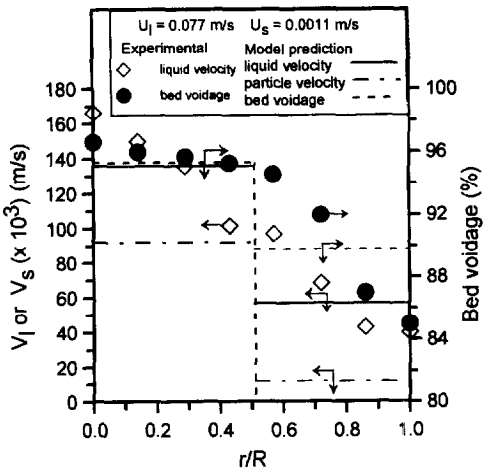

Fig. 2. Comparison of the model prediction and the experimental results of the radial distributions in the liquid velocity and bed voidage under $U_l=0.077$ m s^{-1}, $U_s=0.0011$ m s^{-1} and $\varepsilon=0.914$.

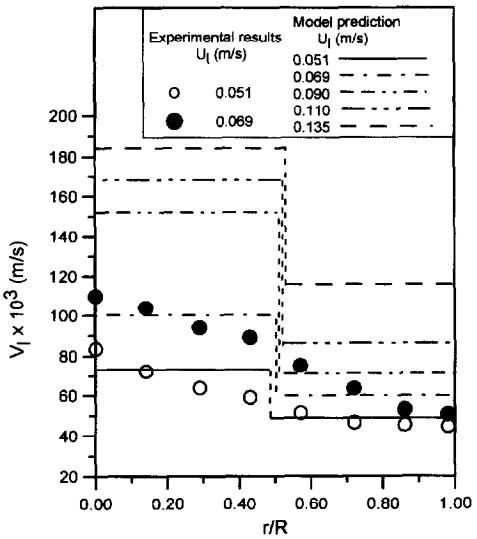

Fig. 3. Comparison of the model predictions and the experimental results of the radial distributions in the liquid velocity under $U_s = 0.0015$ m s^{-1} and different superficial liquid velocities.

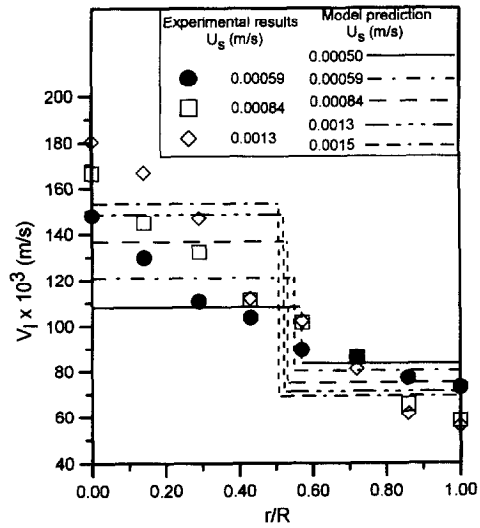

Fig. 4. Comparison of the model predictions and the experimental results of the radial distributions in the liquid velocity under $U_l = 0.09$ m s^{-1} and different particle circulation rates.

operating conditions, although the particle velocity is rather low.

The predicted radial liquid velocity distributions under $U_s = 0.0015$ m s^{-1} and different superficial liquid velocities are presented in Fig. 3. The experimental results under $U_s = 0.0015$ m s^{-1} and $U_l = 0.051$ and 0.069 m s^{-1} are shown in the same figure. It can be seen that the prediction is consistent with the experimental results. The predicted radial liquid velocity distributions under $U_l = 0.09$ m s^{-1} and different particle circulation rates are illustrated in Fig. 4. The comparison with the experimental results under $U_l = 0.09$ m s^{-1} and $U_s = 0.00059$, 0.00084 and 0.0013 m s^{-1} is also given in the same figure. Again, the model predicts the experimental results well.

All the predictions shown in Figs. 2–4 agree very well with the experimental results in the core region, and also provide correct average values in the annular region although they cannot provide exact fit to the measured values given the nature of the core–annulus model. The agreements between the experimental radial profiles of bed voidage and liquid velocity and model predictions indicate that the proposed core–annulus model can be used to simulate the radial non-uniform flow structure in the liquid–solid circulating fluidized bed.

4. Model predictions

With the model properly established, it can now be used to study the effects of the various operating parameters on the flow structure in the fully developed region of the liquid–solid circulating fluidized bed. This would aid the design of such liquid–solid circulating fluidized bed reactors, especially when there are only limited experimental data available.

4.1. Liquid velocity

The predicted liquid velocities under $U_s = 0.0015$ m s^{-1} and different superficial liquid velocities presented in Fig. 3 show that with the increase of superficial liquid velocity, the liquid velocities in both the core and annular regions increase. Fig. 3 also shows that increasing superficial liquid velocity also increases the radial non-uniformity for most situations. To examine the radial non-uniformity, a radial uniformity factor, V_{la}/V_{lc}, is used to illustrate the relative radial distribution of the liquid velocity in the two regions of the bed. When V_{la}/V_{lc} equals 1.0, there is uniform distribution of the liquid velocity in the radial direction. A lower V_{la}/V_{lc} value represents less uniformity in the radial distribution of liquid velocity. The variation of V_{la}/V_{lc} with the increase of superficial liquid velocity is shown in Fig. 5. The results in Figs. 3 and 5 indicate that although the liquid velocities in both the core and annular regions increase with the increase of superficial liquid velocity, the liquid velocity in the core region increases faster than that in the annular region when the superficial liquid velocity increases from 0.051 m s^{-1} to a point between 0.090 m s^{-1} and 0.110 m s^{-1}, resulting in the decrease of the uniformity factor, V_{la}/V_{lc}, that is, resulting in more severe radial non-uniformity. At a point around 0.10 m s^{-1}, V_{la}/V_{lc} reaches the lowest value, indicating that the radial non-uniformity in liquid velocity reaches the maximum (and that the radial uniformity becomes minimum). Beyond this point, with further increase of superficial liquid velocity, it can clearly be seen that the liquid velocity in the annular region increases faster than that in the core region, leading to an increase of V_{la}/V_{lc}, so that the radial non-uniformity in liquid velocity decreases. The liquid velocity at which the radial non-uniformity in liquid velocity reaches the maximum

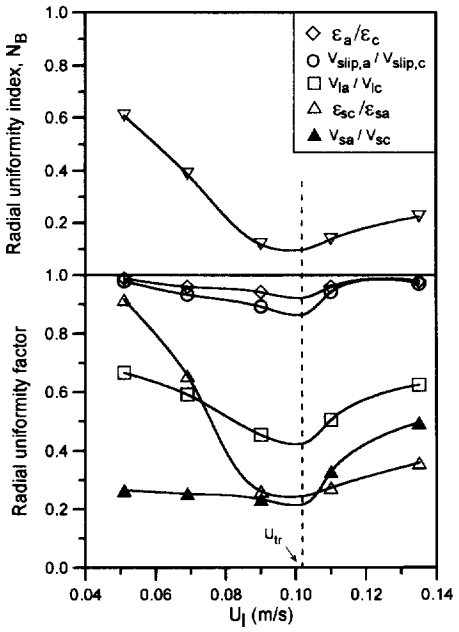

Fig. 5. The variation of the radial uniformity factors and the radial uniformity index with superficial liquid velocity under $U_s = 0.0015$ m s^{-1}.

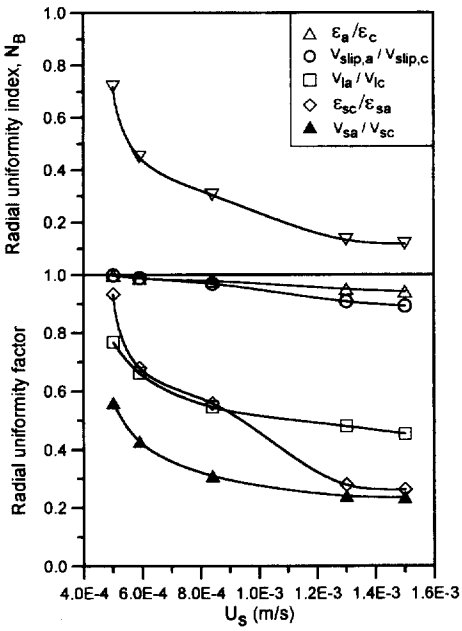

Fig. 6. The variation of the radial uniformity factors and the radial uniformity index with particle circulation rate under $U_l = 0.090$ m s^{-1}.

is defined as the transition velocity, U_a, from the circulating fluidization regime to the liquid transport regime [18].

The predicted liquid velocities in both the core and annular regions under $U_l = 0.09$ m s^{-1} and different particle circulation rates are shown in Fig. 4. The same radial uniformity factor, V_{la}/V_{lc}, is used to characterize the effect of particle circulation rate on the radial flow structure as presented in Fig. 6. With the increase of particle circulation rate, the liquid velocity in the core region increases, while the liquid velocity in the annular region decreases. It can also be easily seen that the magnitude of the variation in the core region is larger than that in the annular region. When the particle circulation rate is rather small, e.g. $U_s = 0.00050$ m s^{-1}, V_{la}/V_{lc} is very close to 1.0, indicating that there is a nearly uniform distribution of the liquid velocity in the radial direction. With the increase of particle circulation rate, V_{la}/V_{lc} decreases monotonically, suggesting that the radial non-uniformity in liquid velocity always increases with particle circulation rate.

4.2. Particle velocity

The predicted particle velocities under $U_s = 0.0015$ m s^{-1} and different superficial liquid velocities are shown in Fig. 7. The radial uniformity factor for the particle velocity distribution (defined as V_{sa}/V_{sc}) is also given in Fig. 5. The particle velocities in the two regions both increase with the increase of liquid velocity. The particle velocity in the core region increases faster than that in the annulus when the superficial liquid velocity is lower than the transition velocity, U_a, so that the radial non-uniformity in the particle velocity increases with the increase of superficial liquid velocity in this range. When the superficial liquid velocity is higher than U_a, due to the faster increase of the liquid velocity in the annular region, the particle velocity in the annular region will increase faster than that in the core region, resulting in the decrease in radial non-uniformity in the particle velocity. The above results also indicate that the variation of the radial non-uniformity in the particle velocity distribution in the bed is consistent with that in the liquid velocity distribution as shown in Figs. 3 and 5.

The particle velocity predicted under $U_l = 0.09$ m s^{-1} and different particle circulation rates is shown in Fig. 8. The comparison of the particle velocities in the two regions is also illustrated in Fig. 6, with the aid of the radial uniformity factor V_{sa}/V_{sc}. With the increase of particle circulation rate, the particle velocity in the core region increases due to the increase of the liquid velocity in this region as shown in Fig. 4, while the particle velocity in the annular region decreases due to the decrease of the liquid velocity in that region. As a result, the radial non-uniformity in the particle

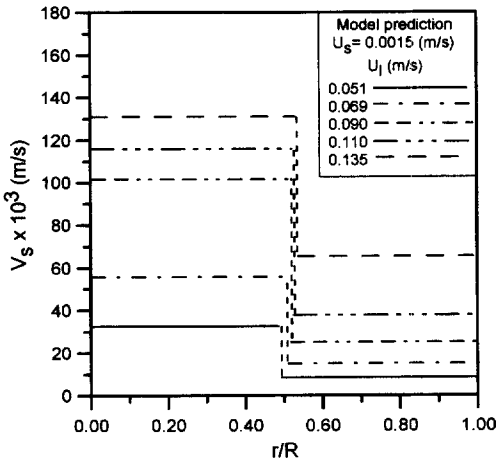

Fig. 7. Predicted radial distributions of the particle velocity under $U_s = 0.0015$ m s^{-1} and different superficial liquid velocities.

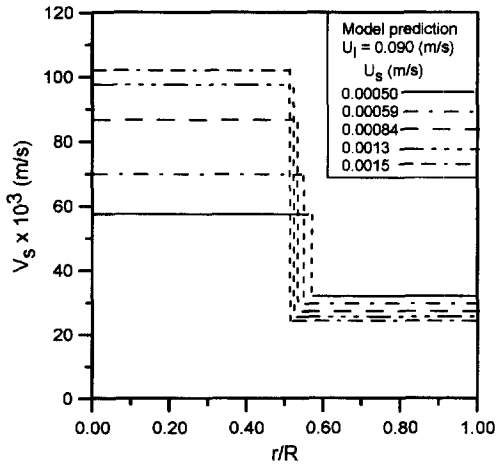

Fig. 8. Predicted radial distributions of the particle velocity under $U_l = 0.09$ m s^{-1} and different particle circulation rates.

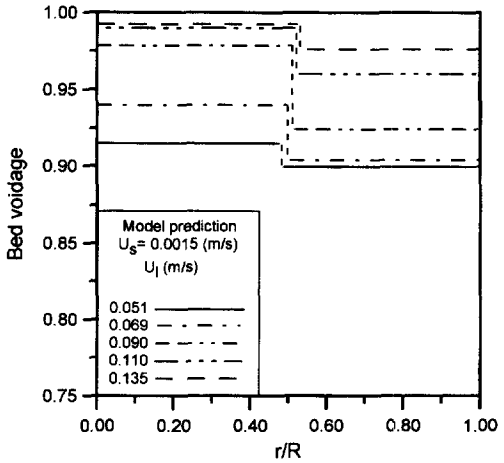

Fig. 9. Predicted radial bed voidage distributions under $U_s = 0.0015$ m s^{-1} and different superficial liquid velocities.

velocity increases with the increase of particle circulation rate, consistent with the variation of the radial non-uniformity in the liquid velocity as shown in Figs. 4 and 6.

4.3. Bed voidage and solids holdup

The variations of the liquid and particle velocities will influence the bed voidages and solids holdups in the two regions. With the increase of superficial liquid velocity, although the liquid and particle velocities in the two regions both increase, the magnitude of the increase in liquid velocity is higher than that of particle velocity. As a consequence, the bed voidage in the two regions increases, as shown in Fig. 9. The variations of the radial uniformity factors of the bed voidage ($\varepsilon_a/\varepsilon_c$) and of the solids holdup ($\varepsilon_{sc}/\varepsilon_{sa}$) in the bed based on the results in Fig. 9 are also illustrated in Fig. 5. With the increase of superficial liquid velocity, the radial non-uniformity in the bed voidage and solids holdup increases first. However, when the superficial liquid velocity is larger than the transition velocity, U_a, as in the cases of the liquid velocity and particle velocity, the radial non-uniformity in the bed voidage and the solids holdup decreases.

Comparing the variations of the radial uniformity values in the liquid velocity, the particle velocity, the bed voidage and the solids holdup presented in Figs. 5, 3, 7 and 9, it can be seen that all radial uniformity factors decrease with the increase of superficial liquid velocity when U_l is less than U_a. At U_a, all radial uniformity factors reach their minimum. Beyond U_a, all radial uniformity factors increase with the increase of superficial liquid velocity. Therefore, it can be concluded that significant change in the flow structure occurs around U_a. This corresponds to the operating regime transition from the circulating fluidization regime to the transport regime reported by Liang et al. [18].

The predicted radial bed voidage distributions under $U_l = 0.09$ m s^{-1} and different particle circulation rates are shown in Fig. 10. The radial uniformity factors of the bed voidage and the solids holdup obtained from the results in Fig. 10 are also presented in Fig. 6. It can be seen that when

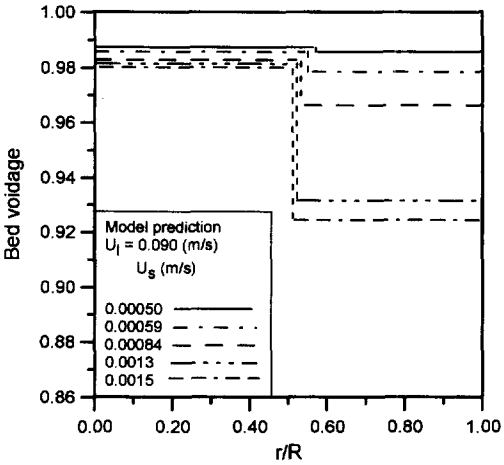

Fig. 10. Predicted radial bed voidage distributions under $U_l = 0.09$ m s^{-1} and different particle circulation rates.

the particle circulation rate is small, e.g. $U_s = 0.00050$ m s^{-1}, the radial uniformity factors of the bed voidage and of the solids holdup are about 1.0, indicating a nearly uniform distribution of the bed voidage and the solids holdup in the radial direction. With the increase of particle circulation rate, the liquid velocity in the core region increases, while the liquid velocity in the annulus decreases, as shown in Figs. 3 and 7. The particle velocity follows the same trend as the liquid velocity, as shown in Figs. 4 and 8. The magnitude of the increase in the liquid velocity in the core region is less than the increase in particle velocity in the same region, making the bed voidage decrease with the increase of particle circulation rate as given in Fig. 10. In the annulus, the decrease in the liquid velocity is higher than the decrease in the particle velocity, resulting in the decrease of bed voidage in the annular region as well. As a consequence, the average bed voidage decreases and the average solids holdup increases with the increase of particle circulation rate. From Figs. 10 and 6, it can also be seen that the radial uniformity in the bed voidage and the solids holdup decrease with the increase of particle circulation rate, indicating an increase in radial non-uniformity.

4.4. Slip velocity

From the predicted liquid velocities and particle velocities of the core and the annular regions, the slip velocities in the two regions can be obtained. Fig. 11 presents the slip velocities in the two regions under $U_l = 0.077$ m s^{-1} and $U_s = 0.0011$ m s^{-1}. The slip velocity, V_{slip}, based on the experimental radial bed voidage distribution, also shown in Fig. 11, is obtained with the assumption that the following equation is valid in each small region containing one measurement point [3]:

$$V_{slip} = U_t \varepsilon^{n-1} \tag{16}$$

It can be seen that the predicted slip velocity with the core–annulus model is consistent with that obtained from the experimental radial bed voidage distribution.

The predicted slip velocities under $U_s = 0.0015$ m s^{-1} and different superficial liquid velocities are presented in Fig. 12. The comparison of the slip velocities in the two regions ($V_{slip,a}/V_{slip,c}$) is also shown in Fig. 5. With the increase of superficial liquid velocity, the slip velocities in the two regions both increase. As with the cases of liquid and particle velocities, when the superficial liquid velocity is less than U_a, the increase in slip velocity in the core region is faster than that in the annulus. Beyond U_a, the increase in slip velocity in the annulus will be faster than that in the core region.

The variations of slip velocities in the core and annulus regions under $U_l = 0.09$ m s^{-1} and different particle circulation rates are shown in Fig. 13. The comparison of the slip velocities in the two regions ($V_{slip,a}/V_{slip,c}$) is given in Fig. 6. It can be seen that with the increase of particle circulation rate, the slip velocities in the two regions will both decrease, as a result of the faster increase in the particle velocity in the core region and the faster decrease in the liquid velocity in the annular region, as shown in Fig. 8. The slip velocity in the annulus decreases faster than that in the core region, resulting in more severe radial non-uniformity in slip velocity.

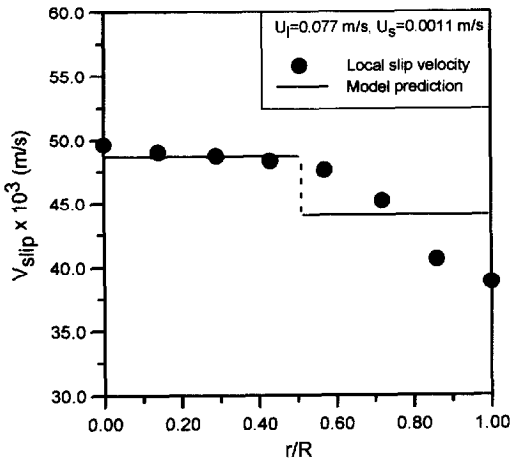

Fig. 11. Comparison of the slip velocities obtained from the core–annulus model and those obtained from the experimental radial bed voidage profile.

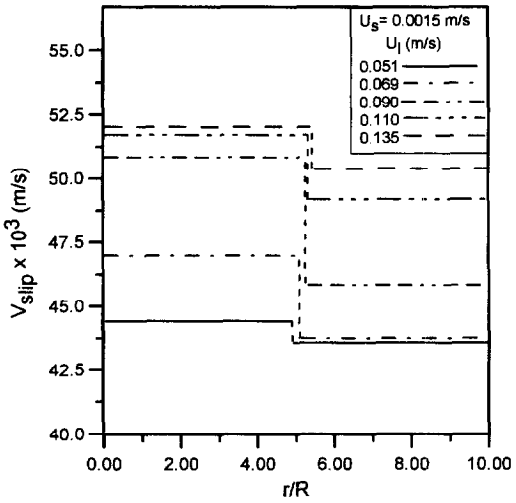

Fig. 12. Predicted radial slip velocity distributions under $U_s = 0.0015$ m s^{-1} and different superficial liquid velocities.

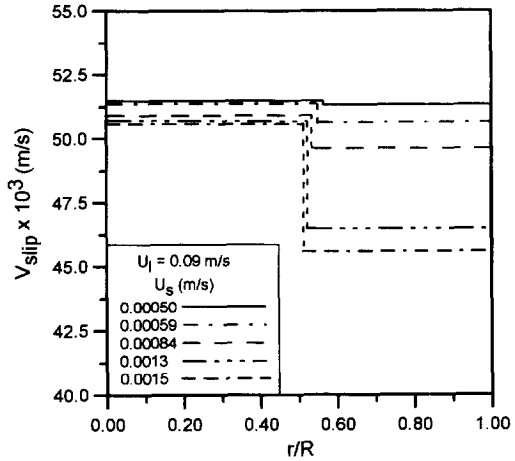

Fig. 13. Predicted radial slip velocity distributions under $U_l = 0.09$ m s^{-1} and different particle circulation rates.

4.5. Drag coefficients

From the predicted liquid and particle velocities, the drag coefficients, C_D, can be obtained with the following equations. In the core region it is

$$(C_D)_c = \frac{4}{3}\frac{d_p(\rho_s - \rho_l)}{\rho_l (V_{lc} - V_{sc})^2} \tag{17}$$

and in the annular region it is

$$(C_D)_a = \frac{4}{3}\frac{d_p(\rho_s - \rho_l)}{\rho_l (V_{la} - V_{sa})^2} \tag{17a}$$

With the assumption that the following equation is valid in each small region containing one measurement point, local relative drag coefficients based on the experimental radial bed voidage profile are obtained:

$$C_D = \frac{4}{3}\frac{Ar}{Re_t^2 \varepsilon^{2n-2}} \tag{18}$$

where

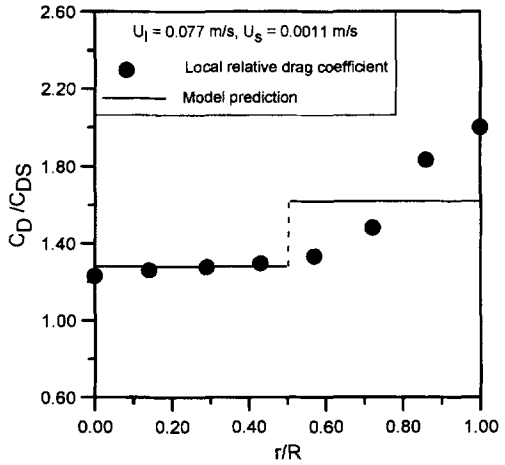

Fig. 14. Comparison of the relative drag coefficients obtained from the core–annulus model with those obtained from the experimental radial bed voidage profile.

$$Ar = d_p^3 \rho_l g(\rho_s - \rho_l)/\mu^2 \tag{19}$$

and

$$Re_t = \frac{U_t d_p \rho_l}{\mu} \tag{20}$$

where d_p is the diameter of the particles and μ is the viscosity of the liquid phase.

Since the drag coefficient, C_D, is a function of the particle shape and concentration, as well as Reynolds number, it is a common practice to first relate C_D to C_{DS}, the drag coefficient of a single spherical particle, with the relative drag coefficient C_D/C_{DS}. For C_{DS}, the following equation for the drag coefficient of the single particle is usually used [22]:

$$C_{DS} = \frac{24}{Re_t} + \frac{3.6}{Re_t^{0.313}} \tag{21}$$

The relative drag coefficients in the core and annular regions under $U_l = 0.077$ m s^{-1} and $U_s = 0.0011$ m s^{-1} obtained from Eqs. (17), (17a) and (21) based on model predictions are presented in Fig. 14. The local relative drag coefficient obtained from Eqs. (18) and (21) based on the experimental radial bed voidage profile is also shown in Fig. 14. It can be seen that the drag coefficients predicted with the core–annulus model agree well with those obtained from the experimental radial bed voidage distribution.

It can be seen from the above results presented in Sections 4.4 and 4.5 that although the correlations based on homogeneous fluidization cannot be used in the whole bed of circulating fluidization due to the radial non-uniformity of the flow structure, these correlations can be used in the core and annulus regions respectively given the assumption of homogeneous fluidization in the two regions. Therefore, the conventional empirical correlations for liquid–solid fluidization are still useful for the circulating fluidization.

4.6. The radius of the core region

The reduced radius of the core region (r_c/R) under different liquid velocities and particle circulating rates is given in Table 1 and also shown in Figs. 3, 4, 7–10. It can be seen that the core region increases with the increase of superficial liquid velocity but decreases with the increase of particle circulating rate. Comparing the core–annulus structure in the gas–solid circulating fluidized beds [13–15], the ratio of the core region in the liquid–solid system is much smaller than that in the gas–solid system. This may be due to the higher viscosity and density of the liquid phase than the gas phase which leads to the higher interaction between the liquid phase and the wall, and therefore a thicker annular region.

5. Radial uniformity index

In the above sections, the radial uniformity in liquid velocity, particle velocity, bed voidage and solids holdup in the bed have been discussed based on the radial flow structure in the LSCFB. In the practical applications of liquid–solid circulating fluidized beds, it is not only the liquid velocity or only the bed voidage that determines the performance of a fluidized bed, since the bed voidage can be controlled independently of the superficial liquid velocity by varying the particle circulation rate. Therefore, it is the combined effect of the above two variables that will determine the flow structure of a liquid–solid circulating fluidized bed. To characterize this combined effect, a radial uniformity index, N_B, is defined here:

$$N_B = \frac{V_{la}/(1-\varepsilon_a)}{V_{lc}/(1-\varepsilon_c)} = \frac{V_{la}}{V_{lc}} \frac{1-\varepsilon_c}{1-\varepsilon_a} \tag{22}$$

Table 1
The reduced radius of the core region under different superficial liquid velocities and particle circulation rates

	U_l (m s^{-1})					U_s (m s^{-1})				
	0.051	0.069	0.090	0.110	0.135	0.00050	0.00059	0.00084	0.0013	0.0015
$U_s = 0.0015$ m s^{-1}										
r_c/R	0.495	0.509	0.520	0.526	0.528					
$U_l = 0.09$ m s^{-1}										
r_c/R						0.571	0.546	0.529	0.524	0.520

In the circulating fluidized bed, since V_{lc} is always higher than V_{la} and ε_c is always higher than ε_a (unless internals are installed to change the flow pattern), the N_B value is less than 1.0, with a lower N_B indicating a less uniform radial flow structure. When the liquid moves downwards in the annular region, N_B will be less than 0.

The physical significance of N_B may be illustrated with a liquid–solid reaction carried out in the liquid–solid circulating fluidized bed reactor, in which the liquid phase is the reactant and the solids phase is the catalyst. When the radial non-uniformity in the liquid (reactant) velocity increases, that is, when V_{la}/V_{lc} decreases, the radial non-uniformity in the residence time distribution of the reactant in the reactor will increase. As a result, the difference in the reactant conversion between the core and annular regions will increase. Therefore, the non-uniformity in the reactant concentration (and the product concentration as well) in the radial direction will increase and the overall reaction conversion will decrease [23]. On the other hand, when the radial non-uniformity in the solids holdup (catalyst holdup) increases, that is, when $(1-\varepsilon_c)/(1-\varepsilon_a)$ decreases, the difference in the reactant conversion between the core and annular regions will increase, because the reaction rate is directly proportional to the catalyst holdup. Hence, the non-uniformity in the reactant concentration in the radial direction will also increase and the overall reaction conversion will decrease. The effect of the radial non-uniformity in the particle (catalyst) velocity is also included in N_B given the relationships among V_{lc}, V_{sc} and ε_c and V_{la}, V_{sa} and ε_a, as shown in Eqs. (1) and (2). Thus, N_B defined in Eq. (22) does reflect the variations of all the key parameters describing the flow structure in the LSCFB. As a result, N_B can be used as an index to characterize the radial uniformity (or non-uniformity) of the flow structure in an LSCFB. If N_B equals 1.0, then there will be uniform radial flow structure in the bed. The smaller the value of N_B is, the more significant is the radial non-uniformity in the bed, and the more significant is the effect of the radial non-uniformity on the performance of the LSCFB reactor. For other kinds of LSCFB applications than catalytic reactions, N_B can also be used as an index to characterize the radial uniformity of the flow structure.

N_B values obtained under different operating conditions are presented in Figs. 5 and 6. The results show that when the superficial liquid velocity is less than U_a, N_B will decrease with the increase of superficial liquid velocity, indicating the increase in the radial non-uniformity of the flow structure. At U_a, N_B reaches the lowest value, so that the radial non-uniformity in the flow structure reaches its maximum value. Beyond U_a, N_B increases with the increase of superficial liquid velocity, indicating the decrease in the radial non-uniformity in the flow structure. With the increase of particle circulation rate, as shown in Fig. 6, N_B decreases, so that the radial non-uniformity of the flow structure increases as well.

6. Flow mechanism in the liquid–solid fluidization system

The above results of the radial non-uniformity in the flow structure in the LSCFB may be explained by the mechanism presented below.

When the liquid flow passes through a packed bed of solids, the packed bed acts as a distributor and the liquid velocity is uniformly distributed radially in the bed, provided that the bottom liquid distributor is designed properly. When the superficial liquid velocity is increased to a value higher than the minimum fluidization velocity but less than the critical velocity for the circulating fluidization (a velocity signifying the transition from conventional liquid–solid particulate fluidization to liquid–solid circulating fluidization as defined by Liang et al. [18]), particles begin to move randomly. This random movement of particles leads to uniform particulate fluidization [6], so that the liquid velocity is uniformly distributed in the radial direction. Since the liquid velocity is still low, the influence of the wall effect is relatively insignificant.

With the increase of superficial liquid velocity, when the superficial liquid velocity is higher than the critical liquid velocity for the circulating fluidization, the bed is operated in the circulating fluidization regime, and a fraction of the particles will be transported out of the bed. At the same time, particles need to be added into the bottom of the bed to maintain a constant solids inventory. Due to the low resistance in the central region of the bed, the liquid velocity in this region will increase faster than that near the wall where the wall friction becomes more significant with the increase of superficial liquid velocity. Therefore, particles in the central region are more likely to be entrained out first. At the same time, with the higher momentum, particles in the central region will have more chance to move into the annulus until an equilibrium is reached with no net exchange between the two regions. As a result, a core–annulus structure with higher liquid velocity, higher particle velocity and higher bed voidage in the core region and lower values of the above parameters in the annular region is established. In this operating regime, with the increase of superficial liquid velocity, the wall factor becomes more significant so that the radial non-uniformity of the flow structure increases.

When the superficial liquid velocity is higher than U_a, that is, when the bed is operated beyond the circulating fluidization regime, with the increase of superficial liquid velocity the solids holdup in the near wall region decreases greatly. Because the shear forces between the particles and the wall are directly proportional to the solids holdup, with the increase of superficial liquid velocity the shear force between the particles and the wall decreases. Therefore, the liquid velocity in the near wall region will increase faster than that in the central region. As a result, the differences in liquid velocity, particle velocity and bed voidage between the two regions will decrease with the increase of superficial liquid velocity, indicating that the fluidized bed begins the transition

from the circulating fluidization regime into the transport regime [18]. With even further increase of the liquid velocity, when the bed enters the transport regime, the flow structure will be uniform again.

With the increase of particle circulation rate, there will be even higher solids holdup in the near wall region. Hence, the friction between the particles and the wall in the near wall region will increase, resulting in a decrease in the liquid velocity and particle velocity in this region. As a consequence, the radial non-uniformity in the flow structure increases.

7. Similarities and differences between gas–solid and liquid–solid systems

Fluidization behaviours of gas–solid (G/S) and liquid–solid (L/S) systems have long been considered different [1] although some attempts have been made to generalize the two systems [4,5]. In conventional low velocity fluidization where no significant particle entrainment occurs, the differences between the two systems are very clear: gas–solid systems are mostly characterized by heterogeneous distribution of particles in the fluidized bed (aggregative fluidization), while liquid–solid systems are regarded as homogeneous with particles uniformly distributed in the bed (particulate fluidization). For high velocity fluidization where particle entrainment becomes very significant and external solids recirculation becomes necessary, however, the differences between the two systems become not so distinct: in both systems, there exist radial non-uniform flow distribution of fluid and particles, with more particles concentrated in the near wall annular region and higher fluid and particle velocities in the central core region. In G/S systems, the heterogeneity decreases as bubbles disappear. On the other hand, the heterogeneity in L/S systems increases with the appearance of radial non-uniformity in the liquid and particle flow structure. This seems to suggest that the two systems become alike when the fluidizing fluid velocity is increased.

In both G/S and L/S circulating fluidization systems, the fluid (gas or liquid) velocity is higher in the central core region than in the annular region and the particle holdup increases from the centre towards the wall, leading to a radial non-uniform flow structure. In addition, particles tend to form some kind of aggregation, although the size of particle clusters in the L/S system is much smaller [24] than that in the G/S system [25]. To maintain continuous operation, particles have to be recirculated and fed back into the bottom of the riser. Solids holdup in the riser can be controlled independently of the fluid velocity by varying the particle circulation rate. On the other hand, there are still clear differences between G/S and L/S systems. For example, the relative size of core region in the L/S system (presented in this work) is much smaller than its counterpart in the G/S system [15]. In addition, the radial non-uniformity is also relatively less significant in the L/S system compared with the G/S system. For example, the uniformity index is in the order of 0.1 for a typical L/S system reported in this work, while it is in the order of -0.01 (there is downflow of fluid phase in the annular region) in a typical G/S system [15]. Therefore, high velocity L/S systems are still more homogeneous than high velocity G/S systems.

8. Conclusions

A core–annulus model is developed to describe the radial non-uniform flow structure in a liquid–solid circulating fluidized bed. The model predictions are consistent with the experimental results in the radial distributions of the bed voidage and the liquid velocities under different superficial liquid velocities and particle circulation rates.

Model predictions show that the bed voidage, the liquid velocity and the particle velocity all increase with the increase of superficial liquid velocity. When the superficial liquid velocity is less than a transition velocity, U_a, the radial non-uniformity of the flow structure increases with the increase of superficial liquid velocity, and beyond U_a, the radial non-uniformity decreases with the increase of superficial liquid velocity. At U_a, the flow structure begins the transition from the circulation fluidization regime to the transport regime. With the increase of particle circulation rate, the liquid and particle velocities increase in the core region, but decrease in the annular region. The bed voidages in the two regions both decrease with the increase of particle circulation rate. The radial non-uniformity of the flow structure increases with the increase of particle circulation rate.

A radial uniformity index has been proposed to characterize the radial flow structure. Defined as $[V_{la}(1-\varepsilon_c)]/[V_{lc}(1-\varepsilon_a)]$, this uniformity index has values lower than 1.0, with a lower value signifying more non-uniform radial flow structure.

From an analysis of the development of the liquid and particle flow, a flow mechanism is proposed for the radial non-uniform flow structure in the liquid–solid circulating fluidized bed. The similarities and differences between gas–solid and liquid–solid systems are also discussed.

Acknowledgements

The financial support of the Natural Science and Engineering Research Council of Canada (NSERC) is gratefully acknowledged.

Appendix A. Nomenclature

Ar	Archimedes number, $d_p^3\rho_l g(\rho_s-\rho_l)/\mu^2$
b	empirical coefficient defined in Eq. (15)
C_D	drag coefficient
C_{DS}	drag coefficient of a single spherical particle

D	diameter of the fluidized bed
f_0	empirical coefficient defined in Eq. (15)
f_{la}	Fanning friction factor between the liquid and the wall
f_{lc}	Fanning friction factor of the liquid phase between the core and the annular regions
f_{sa}	friction factor between the particles and the wall
f_{sc}	friction factor of the solids phase between the core and the annular regions
G_s	particle circulation rate (kg m^{-2} s^{-1})
g	gravity acceleration (ms^{-2})
N_B	radial uniformity index
n	index of the Richardson and Zaki equation
P	pressure (Pa)
R	bed radius (m)
Re_t	Reynolds number at particle terminal velocity, $d_p U_t \rho_l / \mu$
r	radial position (m)
r_c	core region radius (m)
U_a	transition liquid velocity from the circulating fluidization regime to the liquid transport regime (m s^{-1})
U_l	superficial liquid velocity (m s^{-1})
U_s	particle circulation rate expressed as superficial particle velocity (m s^{-1})
U_t	particle terminal velocity (m s^{-1})
V_l	actual liquid velocity (m s^{-1})
V_{la}	actual liquid velocity in the annulus (m s^{-1})
V_{lc}	actual liquid velocity in the core (m s^{-1})
V_{sa}	particle velocity in the annulus (m s^{-1})
V_{sc}	particle velocity in the core (m s^{-1})
V_{slip}	slip velocity between liquid and particles (m s^{-1})
$V_{slip,c}$	slip velocity in the core (m s^{-1})
$V_{slip,a}$	slip velocity in the annulus (m s^{-1})
x	axial distance from the bottom of the bed (m)
ε	average bed voidage
ε_a	voidage in the annulus
ε_c	voidage in the core
ρ_l	liquid density (kg m^{-3})
ρ_s	particle density (kg m^{-3})
τ_{lc}	shear force of the liquid between the core and annular regions (N s^{-1})
τ_{lw}	shear force between the liquid phase and the wall (N s^{-1})
τ_{sc}	shear force of the solids between the core and annular regions (N s^{-1})
τ_{sw}	shear force between particles and the wall (N s^{-1})

Subscripts

a	annulus
c	core
l	liquid
s	particles
w	wall

References

[1] J.P. Couderc, Incipient fluidization and particulate systems, in: J.F. Davidson, R. Clift, D. Harrison (Eds.), Fluidization, 2nd ed., Academic Press, London, 1985, pp. 1–46.

[2] R.D. Felice, Hydrodynamics of liquid fluidization, Chemical Engineering Science 50 (1995) 1213–1245.

[3] J.F. Richardson, W.N. Zaki, Sedimentation and fluidization: part I, Trans. Inst. Chemical Engineers 32 (1954) 35–53.

[4] M. Kwauk, Generalized fluidization, I: steady-state motion, Scientia Sinica 12 (1963) 587–612.

[5] M. Kwauk, Generalized fluidization, II: accelerative motion with steady profiles, Scientia Sinica 13 (1964) 1477–1492.

[6] M. Kwauk, Fluidization: Idealized and Bubbleless, with Application, Science Press and Ellis Horwood, Beijing, 1992.

[7] W.-G. Liang, J.-X. Zhu, Y. Jin, Z.-Q. Yu, Z.-W. Wang, J. Zhou, Radial non-uniformity of flow structure in a liquid–solid circulating fluidized bed, Chemical Engineering Science 51 (1996) 2001–2010.

[8] H. Weinstein, M. Shao, M. Schnitzlein, Radial variation in solid density in high velocity fluidization, in: P. Basu (Ed.), Circulation Fluidized Bed Technology, Pergamon, Toronto, 1986, pp. 201–206.

[9] W. Zhang, Y. Tung, J.E. Johnsson, Radial voidage profiles in fast fluidized beds of different diameters, Chemical Engineering Science 46 (1991) 3045–3052.

[10] B. Herb, S. Dou, K. Tuzla, J.C. Chen, Solid mass fluxes in circulating fluidized beds, Powder Technology 70 (1992) 197–205.

[11] J.L. Sinclair, R. Jackson, Gas–particle flow in a vertical pipe with particle–particle interaction, AIChE Journal 35 (1989) 1473–1486.

[12] D.R. Bai, Y. Jin, Z.Q. Yu, The two-channel model for fast fluidization, in: M. Kwauk, D. Kunii (Eds.), Fluidization '88: Science and Technology, Science Press, Beijing, 1988, pp. 155–164.

[13] F. Berruti, N. Kalogerakis, Modelling the internal flow structure of circulating fluidized beds, Canadian Journal of Chemical Engineering 67 (1989) 1010–1014.

[14] D.R. Bai, J.-X. Zhu, Y. Jin, Z.Q. Yu, Internal recirculation flow structure in vertical upflow gas–solids suspensions, part I: a core–annulus model, Powder Technology 85 (1995) 171–177.

[15] D.R. Bai, J.-X. Zhu, Y. Jin, Z.Q. Yu, Internal recirculation flow structure in vertical upflow gas–solids suspensions, part II: flow structure predictions, Powder Technology 85 (1995) 179–188.

[16] P.A. Ambler, B.J. Milne, F. Berruti, D.S. Scott, Residence time distribution of solids in a circulating fluidized bed: experimental and modelling studies, Chemical Engineering Science 45 (1990) 2179–2186.

[17] H. Kagawa, H. Mineo, R. Yamazaki, K. Yoshida, A gas–solid contacting model for fast fluidized bed, in: P. Basu, M. Horio, M. Hasatani (Eds.), Circulating Fluidized Technology III, Pergamon, Oxford, 1991, pp. 551–556.

[18] W.G. Liang, S.L. Zhang, J.-X. Zhu, Y. Jin, Z.Q. Yu, Z.W. Wang, Flow characteristics of liquid–solid circulating fluidized bed, Powder Technology 90 (1997) 95–102.

[19] R.B. Bird, E.S. Warren, N.L. Edwin, Transport Phenomena, J. Wiley, New York, 1960.

[20] H.E. Rose, R.A. Duckworth, Transport of solid particles in liquids and gases, The Engineer 227 (1969) 392–396, 430–433, 478–483.

[21] R.A. Duckworth, G. Argyros, Influence of density ratio on the pressure gradient in pipes conveying suspensions of solids in liquids, in: H.S.

Stephens, W.A. Thorton (Eds.), Hydrotransport 2: The 2nd International Conference on the Hydraulic Transport of Solids in Pipes, BHRA Fluid Engineering, Bedford, 1972, pp. D1/1–D1/11.

[22] C.Y. Wen, A.F. Galli, Dilute phase system, in: J.F. Davidson, D. Harrison (Eds.), Fluidization, Academic Press, London, 1971, pp. 677–710.

[23] W.G. Liang, J.-X. Zhu, Effect of radial flow non-uniformity on the alkylation reaction in a liquid–solid circulating fluidized bed (LSCFB) reactor, Industrial and Engineering Chemistry Research 36 (12) (1997), in press.

[24] Y.-M. Chen, C.-S. Jang, P. Cai, L.-S. Fan, On the formation of disintegration of particle clusters in a liquid–solid transport bed, Chemical Engineering Science 46 (1991) 2253–2268.

[25] H.T. Bi, J.-X. Zhu, Y. Jin, X.Q. Yu, Forms of particle aggregations in CFB, in: Proc. 6th Chinese National Conf. on Fluidization, Chinese Society of Particuology, Beijing, 1993, pp. 162–167.